Biomech Model Mechanobiol (2011) 10:383–395
DOI 10.1007/s10237-010-0241-7

ORIGINAL PAPER

A hybrid bioregulatory model of angiogenesis during bone fracture healing

Véronique Peiffer · Alf Gerisch · Dirk Vandepitte · Hans Van Oosterwyck · Liesbet Geris

Received: 13 April 2010 / Accepted: 30 June 2010 / Published online: 9 September 2010

Abstract Bone fracture healing is a complex process in which angiogenesis or the development of a blood vessel network plays a crucial role. In this paper, a mathematical model is presented that simulates the biological aspects of fracture healing including the formation of individual blood vessels. The model consists of partial differential equations, several of which describe the evolution in density of the most important cell types, growth factors, tissues and nutrients. The other equations determine the growth of blood vessels as a result of the movement of leading endothelial (tip) cells. Branching and anastomoses are accounted for in the model. The model is applied to a normal fracture healing case and subjected to a sensitivity analysis. The spatiotemporal evolution of soft tissues and bone, as well as the development of a blood vessel network are corroborated by comparison with experimental data. Moreover, this study shows that the proposed mathematical framework can be a useful tool in the research of impaired healing and the design of treatment strategies.

Keywords Bone regeneration · Endothelial cell · VEGF · Partial differential equation · Treatment strategy

V. Peiffer · D. Vandepitte
Division of Production Engineering, Machine design and Automation, Department of Mechanical Engineering, Katholieke Universiteit Leuven, Celestijnenlaan 300B, 3001 Leuven, Belgium
e-mail: dirk.vandepitte@mech.kuleuven.be

Present Address:
V. Peiffer (✉)
Department of Aeronautics, Imperial College London, South Kensington Campus, London SW7 2AZ, UK
e-mail: v.peiffer09@imperial.ac.uk

A. Gerisch
Institut für Mathematik, Martin-Luther-Universität Halle-Wittenberg, 06099 Halle, Saale, Germany

Present Address:
A. Gerisch
Fachbereich Mathematik, Technische Universität Darmstadt, Dolivostrasse 15, 64293 Darmstadt, Germany

H. Van Oosterwyck · L. Geris
Division of Biomechanics and Engineering Design, Department of Mechanical Engineering, Katholieke Universiteit Leuven, Celestijnenlaan 300C, PB 2419, 3001 Leuven, Belgium
e-mail: hans.vanoosterwyck@mech.kuleuven.be

H. Van Oosterwyck · L. Geris
Prometheus, Division of Skeletal Tissue Engineering, K.U. Leuven, Herestraat 48, 3000 Leuven, Belgium

Present Address:
L. Geris (✉)
Biomechanics Research Unit, Université de Liège, Bât. B52/3 Génie biomécanique, chemin des Chevreuils 1, 4000 Liège, Belgium
e-mail: liesbet.geris@ulg.ac.be

1 Introduction

1.1 The process of bone healing including angiogenesis

Bone is a unique tissue because it can heal scarlessly. After trauma, blood clotting induces the formation of a hematoma. This marks the beginning of the first stage of the regeneration process, the "inflammation phase". Due to vascular damage, the trauma site becomes hypoxic, causing cells and tissues to necrose. Inflammatory cells invade the site, followed by fibroblasts, endothelial cells and mesenchymal stem cells (Taguchi et al. 2005). A myriad of growth factors is present in the fracture zone. As the healing process passes into the "reparative phase", fibrous tissue is gradually formed here, resulting in a soft callus. Mesenchymal stem

cells start differentiating, regulated by biological factors and mechanical stimuli (Bostrom 1998; Carter et al. 1998). Close to the undamaged cortical bone, intramembranous ossification occurs. In the central part of the fracture zone, mesenchymal stem cells first differentiate into chondrocytes, as the oxygen tension is too low for osteoblasts to appear (Hirao et al. 2006). After maturation, hypertrophic chondrocytes produce vascular growth factors which attract blood vessels to the cartilaginous tissue. The vasculature restores normoxia and enables endochondral ossification, filling the callus with woven bone. When the fracture ends are connected by a bony callus, clinical union is reached (Marsh 1998). Bone healing concludes with a "remodeling phase", during which woven bone is replaced by lamellar bone and the blood vessel network is reorganized, leading to a recovery of the bone's original shape and size.

Angiogenesis or the development of a blood vessel network in the callus is crucial to successful healing. The exact mechanisms behind this process are not yet fully understood, but the importance of the role of vascular growth factors such as the Vascular Endothelial Growth Factor (VEGF) is generally acknowledged (Street et al. 2002). Cells that are deprived of oxygen produce VEGF. The protein diffuses through the tissue and reaches endothelial cells of nearby blood vessels. Some of these cells react by expressing the "tip cell"-phenotype. Others become "stalk cells". A tip cell has filopodia, by which it can sense microenvironmental stimuli. Guided by these stimuli the tip cell will move away from its mother vessel and give lead to a branch. When the tip cell detects a gradient in the VEGF concentration, it will move toward the source, a process called chemotaxis. As the cell attaches and moves along fibers in the extracellular matrix, there is also a haptotactic component of tip cell motion. The stalk cells do not move independently, but follow the tip by stretching and proliferating steadily. When a growing branch meets another vessel, they undergo anastomosis (De Smet et al. 2009).

1.2 Mathematical models of bone healing and angiogenesis

Computer simulations can shed light on the fracture healing process by testing and comparing different hypotheses on regeneration mechanisms. In silico models can also facilitate the design of treatment strategies for impaired healing, thereby reducing the experimental research cost.

Shefelbine et al. (2005) proposed a fuzzy logic model to simulate fracture healing based on local mechanical factors as described by Claes and Heigele (1999) and the local vascularity. To model the progress of angiogenesis in the fracture callus (by means of a single variable representing the vascularity), a number of basic mechanoregulatory rules were applied. Chen et al. (2009) modified the set of fuzzy logic rules and simulated nutrition supply instead of the vascularity. Geris et al. (2008) proposed a continuous mathematical model of bone regeneration that describes healing in terms of densities of the most important cell types, generic growth factor families and tissues. The process of angiogenesis is modeled through the spatiotemporal evolution of an endothelial cell concentration and a vascular density. Although the predicted ossification process matches experimental observations quite well, a comparison between the experimentally observed and the predicted angiogenic response is not so straightforward. The reason is that the discrete nature of vasculature cannot be fully captured by continuous variables. However, as the continuum level is particularly suited to facilitate comparison of soft tissue and bone formation predictions with histological data, the hybrid modeling approach is the obvious solution. In addition to continuous variables, a hybrid model contains a discrete variable that indicates the presence or absence of a blood vessel at a specific location. A number of hybrid mathematical models have been developed describing angiogenesis, mostly in relation to tumor growth. Anderson and Chaplain (1998) modeled the tip cell motion as a probabilistic biased random walk, a lattice-based approach that is also followed in the hybrid bone regeneration model of Checa and Prendergast (2008). The deterministic hybrid model of Sun et al. (2005) associates a set of partial differential equations with each tip cell to define the velocity of the cell. Milde et al. (2008) presented a similar method to determine the acceleration of the tip cells. All these models assume branching to be the result of the division of a tip cell, which is incorrect given recent advances in the understanding of angiogenesis (De Smet et al. 2009). Qutub and Popel (2009) recently proposed a rule-based model of sprouting angiogenesis that takes these insights into account. It furthermore explicitly simulates the elongation and proliferation of stalk cells and the effect of Notch factor production.

1.3 Objectives of this study

In this study, we propose a deterministic hybrid modeling framework for bone regeneration including angiogenesis based on the work of Geris et al. (2008); Sun et al. (2005) and Qutub and Popel (2009). Results are corroborated by comparison with experimental data from literature. Sensitivity of the model outcome to the newly introduced parameters is evaluated. To demonstrate its potential, the model is applied to simulate both normal and impaired healing cases, as well as to design potential treatment strategies for the latter.

2 Materials and methods

2.1 Evolution of continuous variables

The hybrid fracture healing model presented in this study is built on the continuous model of Geris et al. (2008), which

describes fracture healing as the spatiotemporal variation in density of 12 variables: mesenchymal stem cells (c_m), fibroblasts (c_f), chondrocytes (c_c), osteoblasts (c_b), endothelial cells (c_v), fibrous extracellular matrix (m_f), cartilaginous extracellular matrix (m_c), bone extracellular matrix (m_b), vascular matrix (m_v) and generic osteogenic (g_b), chondrogenic (g_c) and vascular (g_v) growth factors. To be able to represent individual blood vessels, the continuous variable c_v is changed into a discrete variable c_v in this study and the vascular matrix density m_v is omitted. The evolution of each of the continuous variables is described by a partial differential equation (PDE) of the taxis-diffusion-reaction type:

$$\frac{\partial c_m}{\partial t} = \nabla \cdot \big(D_m \nabla c_m - C_{m_{\mathrm{CT}}} c_m \nabla (g_b + g_v) - C_{m_{\mathrm{HT}}} c_m \nabla m\big) + A_m c_m (1 - \alpha_m c_m) - F_1 c_m - F_2 c_m - F_4 c_m \quad (1)$$

$$\frac{\partial c_f}{\partial t} = \nabla \cdot \big(D_f \nabla c_f - C_f c_f \nabla g_b\big) + A_f c_f (1 - \alpha_f c_f) + F_4 c_m - F_3 d_f c_f \quad (2)$$

$$\frac{\partial c_c}{\partial t} = A_c c_c (1 - \alpha_c c_c) + F_2 c_m - F_3 c_c \quad (3)$$

$$\frac{\partial c_b}{\partial t} = A_b c_b (1 - \alpha_b c_b) + F_1 c_m + F_3 c_c - d_b c_b \quad (4)$$

$$\frac{\partial m_f}{\partial t} = P_{\mathrm{fs}} (1 - \kappa_f m_f) c_f - Q_f m_f m_c c_b \quad (5)$$

$$\frac{\partial m_c}{\partial t} = P_{\mathrm{cs}} (1 - \kappa_c m_c) c_c - Q_c m_c c_b \quad (6)$$

$$\frac{\partial m_b}{\partial t} = P_{\mathrm{bs}} (1 - \kappa_b m_b) c_b \quad (7)$$

$$\frac{\partial g_c}{\partial t} = \nabla \cdot \big(D_{\mathrm{gc}} \nabla g_c\big) + E_{\mathrm{gc}} c_c - d_{\mathrm{gc}} g_c \quad (8)$$

$$\frac{\partial g_b}{\partial t} = \nabla \cdot \big(D_{\mathrm{gb}} \nabla g_b\big) + E_{\mathrm{gb}} c_b - d_{\mathrm{gb}} g_b \quad (9)$$

$$\frac{\partial g_v}{\partial t} = \nabla \cdot \big(D_{\mathrm{gv}} \nabla g_v\big) + E_{\mathrm{gvb}} c_b + E_{\mathrm{gvc}} c_c - g_v (d_{\mathrm{gv}} + d_{\mathrm{gvc}} c_v) \quad (10)$$

where $m (= m_f + m_c + m_b)$ represents the total tissue density. The processes described by these equations are schematically illustrated in Fig. 1 and extensively discussed by Geris et al. (2008). Remark that chemotaxis of osteoblasts has been omitted in the work presented here, as a sensitivity analysis for the previous model showed that the influence of this term was negligible.

As a tool to account for influences of oxygen and nutrients, a new variable is added to the set of continuous variables. This variable n is a measure for the concentration of oxygen and nutrients and its evolution is given by:

$$\frac{\partial n}{\partial t} = \nabla \cdot (D_n \nabla n) + E_n c_v - d_n n \quad (11)$$

where the first term on the right-hand side represents the diffusion of oxygen and nutrients, the second term expresses

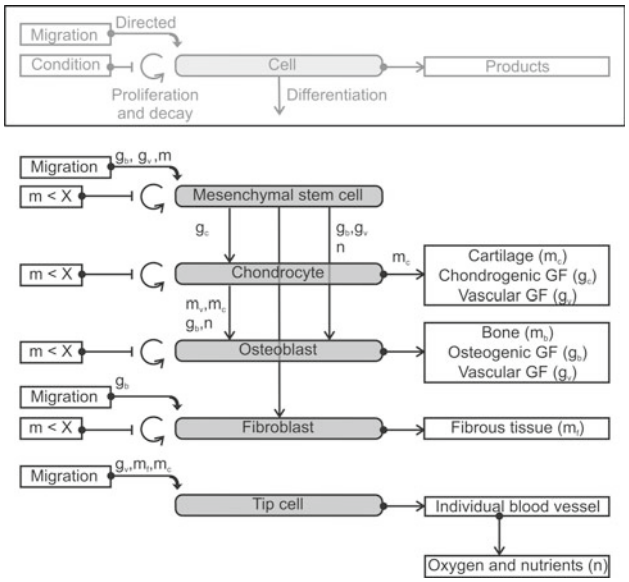

Fig. 1 Schematic overview of the hybrid model. *GF* growth factor, $m = m_f + m_c + m_b$ = total tissue density, X maximum tissue density allowing for proliferation. The involvement of a variable in a regeneration subprocess is indicated by showing the name of that variable next to the arrow representing that particular subprocess

release of oxygen and nutrients from the blood vessels and the last term accounts for the global effect of oxygen/nutrient consumption. The interaction of the additional variable (n) with the other variables is shown in Fig. 1.

The nondimensionalized parameters and variables of all 11 equations are listed in the appendix. Model parameters were derived from in vitro and in vivo experiments as described by Geris et al. (2008). Parameters for which no experimental values were available were estimated taking into account the results of a mathematical stability analysis and corroborated by comparison with the normal healing of a rodent femoral fracture (Harrison et al. 2003). The functional forms related to migration (D_m, $C_{m_{\mathrm{CT}}}$, $C_{m_{\mathrm{HT}}}$, C_f), proliferation (A_m, A_f, A_c, A_b), chondrogenic differentiation (F_2) and osteogenic and chondrogenic growth factor production (E_{gc}, E_{gb}) were taken from Geris et al. (2008). They are briefly described in the appendix. Functional forms related to osteogenic differentiation and vascular growth factor production were adapted to account for the influence of oxygen and nutrients, as discussed below.

The differentiation of mesenchymal stem cells toward osteoblasts is mathematically given by the following functional form:

$$F_1 = \left(\frac{Y_{11} g_b}{H_{11} + g_b} + \frac{Y_{11} g_v}{H_{12} + g_v}\right) \cdot \frac{Y_{12} n^6}{I_v^6 + n^6} \quad (12)$$

in which the factor between brackets expresses that the differentiation is mediated by the presence of both osteogenic and angiogenic growth factors (Street et al. 2002; Mayer et al.

2005; Midy and Plouet 1994). For high chemical concentrations, a saturation effect is modeled to take place. According to the last factor in Eq. 12, the intramembranous ossification rate is taken to depend on the availability of oxygen and nutrients for low oxygen/nutrient concentrations. The sixth-order form used in this factor (and later in Eqs. 13–16) is a commonly employed approach to mathematically describe a switch pattern (Bailón-Plaza and Van der Meulen 2001; Geris et al. 2008), in this case indicating that intramembranous ossification can only take place when the concentration of oxygen and nutrients is sufficiently high.

Endochondral ossification is modeled in the same way as in Geris et al. (2008), except for the necessity of oxygen and nutrients which is taken into account explicitly here:

$$F_3 = \frac{m_c^6}{B_{ec}^6 + m_c^6} \cdot \frac{Y_3 g_b}{H_3 + g_b} \cdot \frac{n^6}{B_v^6 + n^6}. \tag{13}$$

The first factor of Eq. 13 expresses that only hypertrophic chondrocytes play a part in the endochondral ossification process. The model assumes transition of chondrocytes to the hypertrophic phenotype when the cartilage matrix reaches a certain density Geris et al. (2008). The other factors express the need of osteogenic growth factors (second factor) and oxygen and nutrients (last factor).

Angiogenic growth factors are produced by osteoblasts and hypertrophic chondrocytes. The functional forms describing their production rate are:

$$E_{\mathrm{gvb}} = \frac{G_{\mathrm{gvb}} H_{\mathrm{gv}}^6}{H_{\mathrm{gv}}^6 + g_v^6} \cdot \frac{K_n^6}{K_n^6 + n^6} \tag{14}$$

$$E_{\mathrm{gvc}} = \frac{G_{\mathrm{gvc}} H_{\mathrm{gv}}^6}{H_{\mathrm{gv}}^6 + g_v^6} \cdot \frac{K_n^6}{K_n^6 + n^6} \cdot \frac{m_c^6}{B_{ec}^6 + m_c^6} \tag{15}$$

where the first two factors in each equation describe that the angiogenic growth factor production rate is high for low angiogenic growth factor and oxygen/nutrient concentrations. The last factor of Eq. 15 ensures that only hypertrophic chondrocytes contribute to the angiogenic growth factor production.

Finally, E_n, which is new compared to the continuous model of Geris et al. (2008), expresses that blood vessels release oxygen and nutrients:

$$E_n = \frac{G_n H_n^6}{H_n^6 + n^6}. \tag{16}$$

2.2 Mathematical description of angiogenesis

Blood vessels are represented by a discrete variable c_v. When a grid volume contains a vessel, the variable is set to 1, otherwise $c_v = 0$. This implies that, although the movement of the tip cell itself is independent of the chosen grid (see below), the vessel diameter is defined by the grid resolution in its current implementation. The evolution of c_v is determined by blood vessel growth, branching and anastomoses.

Blood vessel growth To describe the growth of a blood vessel, the model computes the movement of the corresponding tip cell. In analogy to the approach of Sun et al. (2005), this is accomplished by solving tip cell velocity equations of the form:

$$\frac{\mathrm{d}\mathbf{x}_t}{\mathrm{d}t} = v_t \frac{\mathbf{u}_t}{\|\mathbf{u}_t\|_2} \tag{17}$$

where $\mathbf{x}_t$ represents the position, v_t the speed and $\mathbf{u}_t$ the direction of movement of the tip cell. The tip cell speed depends on the VEGF concentration (De Smet et al. 2009). For VEGF concentrations below g_v^*(10 ng/ml), blood vessels do not grow (Bernatchez et al. 1999). The tip cells move faster for higher VEGF concentrations up to a maximum speed of $v_t^{\max}$[35 µm/day, value chosen in the range suggested by Sun et al. (2005)]. This is mathematically described as:

$$v_t = \begin{cases} 0 & \text{if } g_v < g_v^* \\ v_t^{\max} \frac{g_v^6}{g_v^6 + (g_v^*)^6} & \text{if } g_v \geq g_v^*. \end{cases}$$

Tip cells are guided by chemotaxis and haptotaxis. In this approach, the presence of collagen fibers in the extracellular tissue is explicitly modeled. Cells are assumed to always try to move along the fibers that are present in the tissue. This results in the following description of the direction of tip cell movement:

$$\mathbf{u}_t = K\left(k_c \nabla g_v + k_h \nabla (m_f + m_c)\right) \tag{18}$$

with $k_c = 1 - k_h$. In this study the chemotactic coefficient k_c and haptotactic coefficient k_h are both set to 0.5, in the assumption that chemical and matrix gradients are equally important. The matrix K is defined as:

$$K = \begin{pmatrix} 1 & 0 \\ 0 & 1 \end{pmatrix} + k_a \begin{pmatrix} -v_y^2 & v_x v_y \\ v_x v_y & -v_x^2 \end{pmatrix} \tag{19}$$

where the unit vector (v_x, v_y) determines the orientation of the matrix fibers and parameter k_a is a measure for the influence of the fiber orientation on the growth direction of blood vessels. The k_a-value can vary between 0 (zero influence) and $k_a^{\max}$ ($\leq$1 in general, chosen to equal 1 in this study for a maximal influence). As both k_a and the fiber orientation can randomly vary throughout the domain, the model is able to account for the variable nature of the angiogenic process. Fig. 2a, b, demonstrates the migration of tip cells and the blood vessel growth at two different time points.

Branching New tip cells can be recruited if the VEGF concentration is high (above g_v^*). Along the vessels the model selects positions that can deliver a tip cell. The potential tip cell positions are at intervals of 100 µm on the mother vessels, leading to the formation of a network in which the maximal separation between a cell and a vessel is 50 µm. This

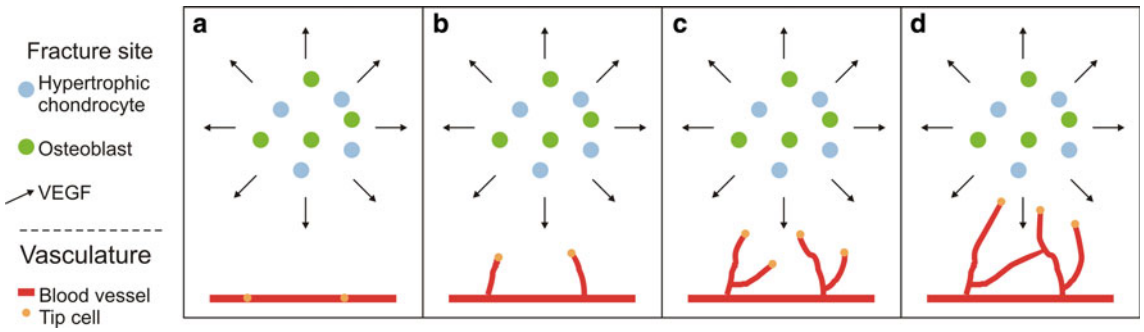

Fig. 2 The process of angiogenesis; **a** presence of a blood vessel in the neighborhood of the fracture zone in which different cells produce VEGF; **b** blood vessel growth as a result of tip cell movement. Only the chemotactic component is illustrated; **c** branching through the selection of new tip cells in existing vessels; **d** anastomosis formation

assures sufficient supply of oxygen and nutrients to all cells (Carmeliet and Jain 2000). A branch will only be created if the movement direction of the new tip cell differs enough from the orientation of its mother vessel (threshold chosen at a 24° angle based on the results of a mathematical stability analysis). Between subsequent branching events, the model foresees at least 3 healing days. The branching process is schematically depicted in Fig. 2c where two new tip cells have been selected, resulting in two branches on the growing blood vessels.

Anastomosis In Fig. 2d, an anastomosis has developed. This occurs when a tip cell encounters a blood vessel or, mathematically, when the tip cell reaches a grid volume where $c_v = 1$. After this event, the cell will no longer be considered as a tip cell.

2.3 Implementation details

The method of lines is applied to all PDEs. As mass conservation of the continuous variables is highly important, a finite volumes approach in space is used (Gerisch and Chaplain 2006). The equations are solved on a 2D grid with a grid cell size of 25 µm. The spatial discretization scheme guarantees nonnegativity of the continuous variables and is globally of order 2 (Gerisch and Chaplain 2006). Time integration of the resulting ordinary differential equations (ODE) is done using a MATLAB Mex interface to the time integration scheme ROWMAP, a ROW-code of order 4 with Krylov techniques for large stiff ODEs (Weiner et al. 1997). After each time step for the continuous variables, the tip cell velocity equations are solved in a few steps using a central difference scheme in space in combination with explicit Euler time integration. The set of tip cells is regularly refreshed to account for anastomoses and branching. The model is implemented in MATLAB (The MathWorks, Natick, MA).

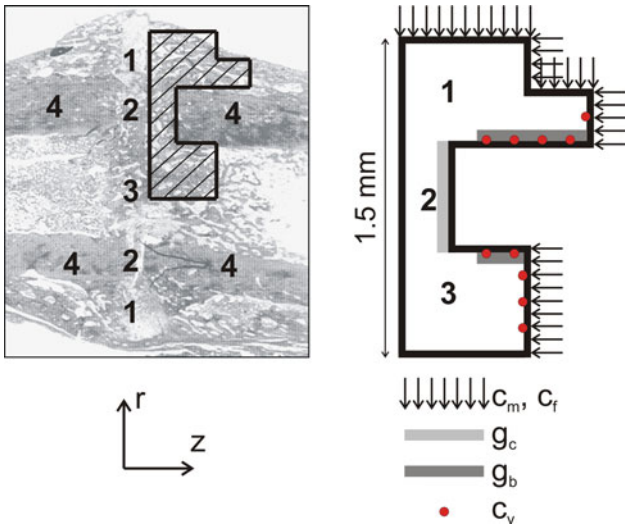

Fig. 3 *Left* Geometrical domain deduced from the real callus geometry at postfracture week 3 (Harrison et al. 2003); *1* periosteal callus; *2* intercortical callus; *3* endosteal callus; *4* cortical bone. *Right* Boundary conditions; c_m: mesenchymal stem cells; c_f: fibroblasts; g_c: chondrogenic growth factors; g_b: osteogenic growth factors; c_v: endothelial cells

2.4 Simulation details

Simulations are conducted utilizing high-performance computational resources provided by the Katholieke Universiteit Leuven, http://ludit.kuleuven.be/hpc.

Normal fracture healing The hybrid model is applied on a spatial domain that is deduced from the real callus geometry of a standardized femoral rodent fracture (Harrison et al. 2003). Because of symmetry, the simulation domain is reduced to one-fourth of the cross-section (see Fig. 3).

The choice of boundary conditions is based on the values used in Geris et al. (2008). No-flux boundary conditions are assumed for all variables, except for those depicted in Fig. 3. Mesenchymal stem cells and fibroblasts are released

into the callus tissue from the periosteum, surrounding soft tissues and the bone marrow [$c_m^{\mathrm{bc}} = 2 \times 10^4$ cells/ml and $c_f^{\mathrm{bc}} = 2 \times 10^4$ cells/ml during the first 3 postfracture days (Gerstenfeld et al. 2003)]. The degrading bone ends are a source of chondrogenic growth factors [$g_c^{\mathrm{bc}} = 2\,\mu$g/ml during the first 5 postfracture days (Barnes et al. 1999)]. The cortex is modeled to deliver osteogenic growth factors [$g_b^{\mathrm{bc}} = 2\,\mu$g/ml during the first 10 postfracture days (Dimitriou et al. 2005)]. The starting positions of the tip cells are shown in Fig. 3. Endothelial cells can leave the domain freely. At symmetry boundaries, this behavior can be seen as the occurrence of an anastomosis of the blood vessel with its mirror vessel. The initial callus consists of fibrous tissue ($m_f^{\mathrm{init}} = 10\,$mg/ml).

Convergence and sensitivity analyses The influence of the explicit Euler time step size is traced by varying its maximum possible value in a simulation from 72 min to 7.2 min and 14.4 h. To check convergence, the grid cell size is changed to double (50 µm) and half (12.5 µm) of its original value (25 µm).

Sensitivity to the orientation of matrix fibers is tested by comparing the results of 10 simulations. Also the influence of horizontal and of vertical fiber alignment are investigated. Simulation results with varying initial tip cell density are compared, and the importance of chemotaxis versus haptotaxis is evaluated by changing the ratio of k_c to k_h. Simulated k_c/k_h ratios are 1/0, 0.75/0.25, 0.5/0.5, 0.3/0.7 and 0.1/0.9.

Impaired fracture healing and treatment strategies A shortage in matrix metalloproteinase 9 (MMP9) in regenerating bone tissue leads to a decrease in the biologically available VEGF concentration (Colnot et al. 2003). This effect is implemented in the model by reducing the VEGF production of hypertrophic chondrocytes (related parameter $G_{\mathrm{gvc}} \times 0.01$). Various treatment strategies were investigated in silico, including daily biologically active VEGF bolus injections ($g_v + 1\,\mu$g/ml in the entire domain) and the administration of an injectable slow release VEGF carrier in the soft tissues surrounding the fracture site [boundary condition of 1 µg/ml, time constant of 5 days (Seeherman et al. 2003)]. Both therapies are started 3 weeks after fracture induction, assuming this is when the impaired healing is diagnosed.

3 Results

3.1 Normal fracture healing

The hybrid model predicts the evolution of the tissue densities in the callus during normal fracture healing, as illustrated in Fig. 4. Mesenchymal stem cells, fibroblasts and growth factors enter the callus from the surrounding tissues.

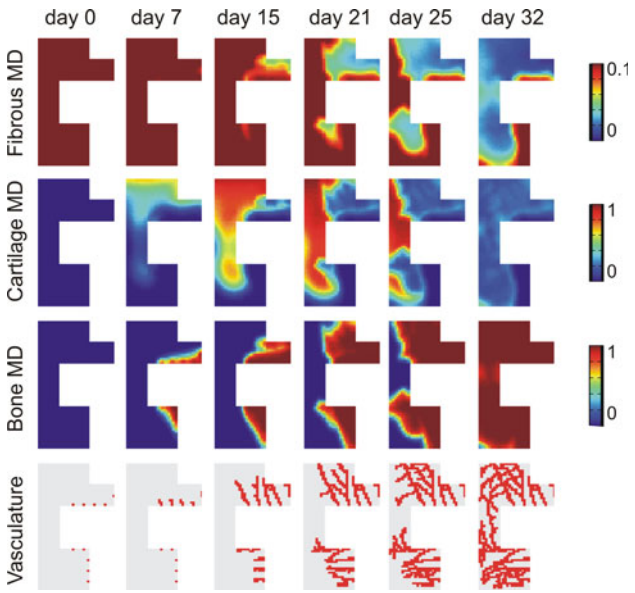

Fig. 4 Normal fracture healing: predicted spatiotemporal evolution of fibrous tissue, cartilage and bone matrix density (MD, ×0.1 g/ml) and of the vasculature

Under the influence of osteogenic growth factors, mesenchymal stem cells near the cortex and away from the fracture line differentiate into osteoblasts, leading to rapid intramembranous ossification. In the remainder of the callus mesenchymal stem cells differentiate into chondrocytes guided by chondrogenic growth factors. When the cartilage reaches a threshold density, around postfracture week (PFW) 1, chondrocytes become hypertrophic and start producing vascular growth factors. This is the onset of angiogenesis. The first blood vessels appear in the periosteal callus. After 1 week, the surface fraction of blood vessels in the callus is 1.8%. In the endosteal callus angiogenesis starts 1 week later; the surface fraction of blood vessels in the total callus then equals 8.1% (PFW 2). The vasculature delivers the necessary oxygen and nutrients for endochondral ossification, gradually filling the fracture zone with bone, while the cartilage degrades. During this process also the fibrous tissue density decreases. Meanwhile, blood vessels continue growing into the callus and creating branches, resulting in a network that can supply the complete fracture zone. The surface fraction of blood vessels in the callus increases to 19.9% (PFW 3), 38.4% (PFW 4) and 41.0% (PFW 5). The reparative healing phase of the rodent femoral fracture takes 4–5 weeks.

Figure 5 compares the experimentally measured temporal evolution of the tissue fractions (Harrison et al. 2003) in the periosteal, intercortical and endosteal callus with the predictions of Geris et al. (2008) and with the results of the new hybrid model. For both models the general trends are in agreement with the experimental data. Throughout the heal-

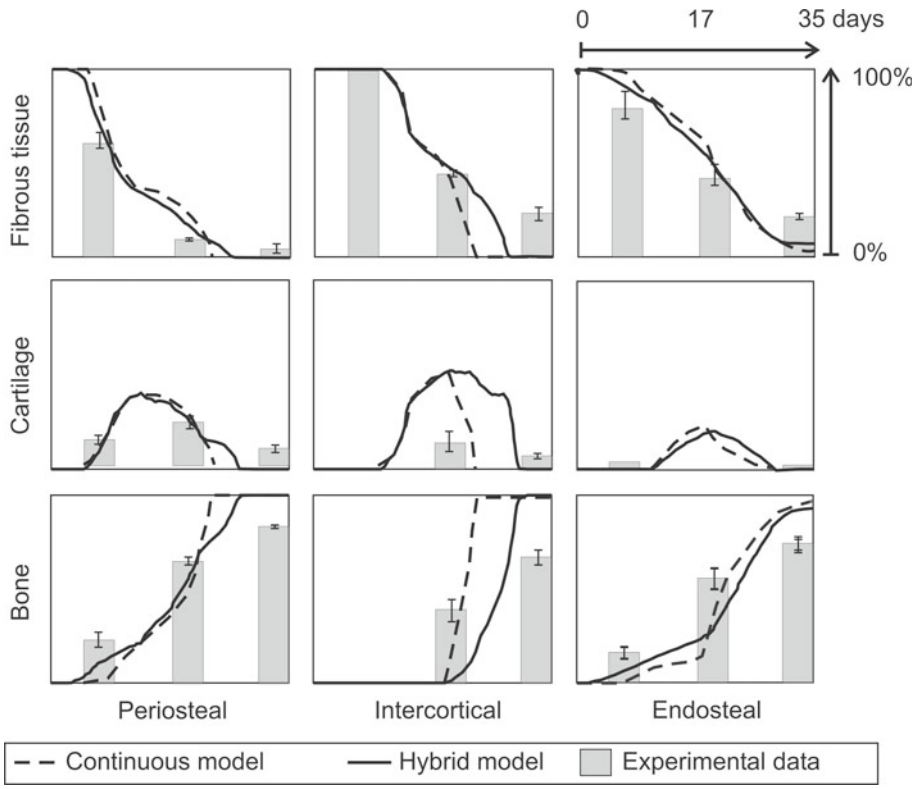

Fig. 5 Normal fracture healing: temporal evolution of the bone, cartilage and fibrous tissue fractions (%) in the periosteal, intercortical and endosteal callus as predicted using the continuous model of Geris et al. (2008) and the newly developed hybrid model and as measured by Harrison et al. (2003)

ing process the bone tissue fraction gradually increases, while fibrous tissue disappears. The cartilage fraction first rises and declines afterward.

3.2 Convergence and sensitivity analyses

A convergence and a sensitivity analysis have been conducted to further evaluate the behavior of the hybrid fracture healing model. The model appears to be robust for changes to the explicit Euler time step size used to advance the tip cell locations. There is a grid dependence though, as the blood vessel diameter is coupled to the grid cell size. This effect is illustrated in Fig. 6. A grid refinement (Fig. 6b, c) will result in a decreased release of oxygen and nutrients causing an initial delay in the healing process. The reversed reasoning holds for grid coarsening (Fig. 6b, a).

Also the influences of tissue fibers, tip cell selection and tip cell movement on the simulation results have been investigated. For 10 simulations the mean blood vessel density at PFW 5 is 39.9%, with a standard deviation of 2.9% caused by the random character of the fiber orientation. An example of a blood vessel network at this point in time can be found in Fig. 7a. When fiber alignment is introduced, the blood vessels seem to follow this structure, as is clear from Fig. 7a for fiber orientations parallel and perpendicular to the bone marrow channel. The results depicted in Fig. 7b show that the initial tip cell density mainly influences the blood vessel network in the proximal and distal areas (away from the fracture line). However, its influence on the blood vessel network and the progression of the fracture healing process is very limited with complete healing in 5 weeks for all cases, as long as the blood vessels possess their full functionality (i.e. nutrient/oxygen providing capacity). Sensitivities involving tip cell movement show that chemotaxis and haptotaxis steer the tip cells in more or less the same directions, provided a minimum amount of chemotaxis. This effect is illustrated in Fig. 8, on which can be seen that the evolution of the vasculature is very similar for k_c-values ranging from 0.3 to 1. However, if the importance of chemotaxis is further reduced ($k_c = 0.1$), some of the blood vessels do not manage to invade the callus. Finally, simulations show that the reactivity of tip cells upon the presence of VEGF is crucial to angiogenesis. A change in the value of the threshold for tip cell motion g_v^*, introduced in Sect. 2.2, leads to results similar to the effect of an impaired fracture healing, as presented in Sect. 3.3.

3.3 Impaired fracture healing and treatment strategies

Figure 9a shows the predicted fracture healing for an MMP9 deficient fracture. The angiogenic response is clearly impaired. The ossification process follows this tendency leading to the delayed formation of ill vascularized bone tissue.

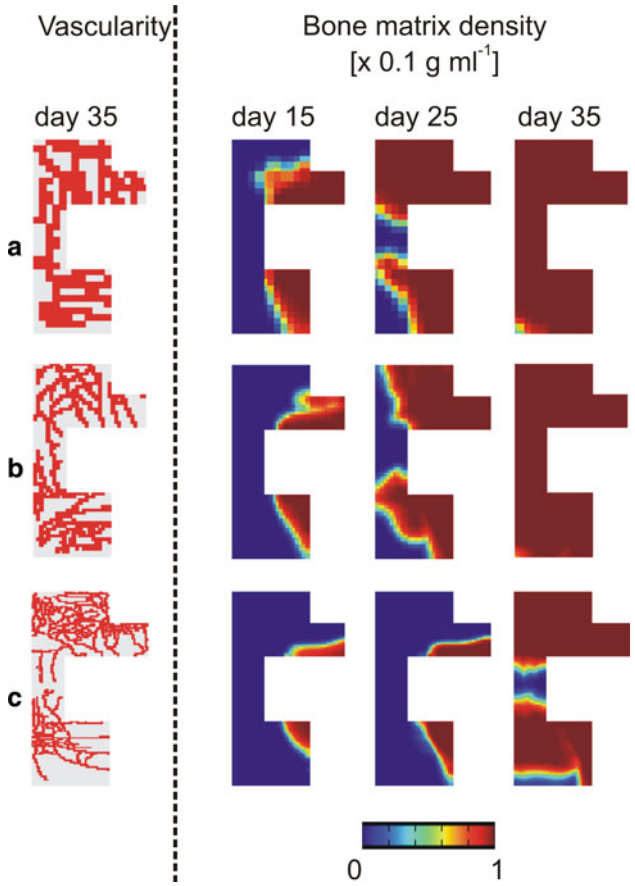

Fig. 6 Influence of the grid cell size, illustrated by the vasculature (*left*) at 35 days and the bone matrix density (*right*) at 5, 15 and 35 days after fracture induction; **a** grid cell size of 50 µm; **b** grid cell size of 25 µm; **c** grid cell size of 12.5 µm

In Fig. 9b the result of a treatment comprising daily bolus VEGF injections is presented. These injections do not seem to have a substantial influence on the progression of healing. Contrarily, making use of an injectable slow release VEGF carrier leads to a speedup of the angiogenic process, as shown in Fig. 9c. Although the predicted blood vessel network is still not fully developed at PFW 5, a clinical union is reached.

Figure 10 summarizes the predicted temporal evolution of tissue fractions and blood vessel density (surface occupied by blood vessels as a percentage of the total callus surface) for the four simulated fracture healing cases.

4 Discussion

4.1 Normal fracture healing

The presented hybrid bone regeneration model is able to capture the essential features of normal fracture healing. Bone appears through intramembraneous and endochondral ossification, the fibrous tissue fraction goes down throughout the healing process and the cartilage fraction increases first to drop afterward. Experimental observations indicate that the ossification starts in the periosteal and the endosteal callus (Harrison et al. 2003), as is the case in the simulation results. Only the predicted delay with which bone formation starts in the intercortical zone is too long. Nevertheless, the evolution of the ossification process in this region is more realistic compared to the results of the continuous model of Geris et al. (2008). Although already slower than the evolution according to the continuous model, the healing process predicted by the hybrid model evolves faster than what is experimentally observed by Harrison et al. (2003). A possible explanation is that the time cells need to mature is not incorporated in the models. For both the continuous and the hybrid model, the qualitative cartilage evolution is in agreement with experimental data (Harrison et al. 2003), but the predicted cartilage density is unnaturally high. The reason might be that the models do not take into account the necessity for oxygen and nutrients to the cartilage production process. As oxygen and nutrients are represented by a variable in the new mathematical framework this can be modified in future versions of the model.

A major advantage of the hybrid model is that the development of the vasculature can be corroborated by comparison with experimental observations. Duvall et al. (2007) present vessel density measurements at PFW 1 and PFW 2 for a

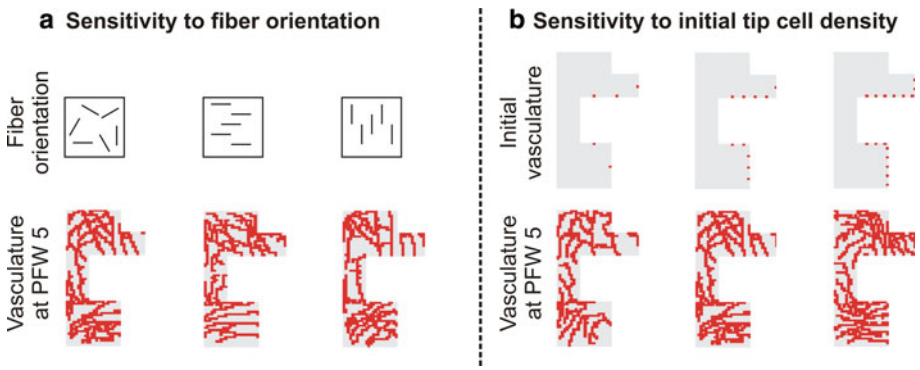

Fig. 7 Sensitivity to fiber orientation and initial tip cell density; **a** sensitivity of the blood vessel network at postfracture week 5 (*bottom row*) to the orientation of matrix fibers (*top row*); **b** sensitivity of the blood vessel network at postfracture week 5 (*bottom row*) to the number of tip cells selected at the start of the healing process (*top row*)

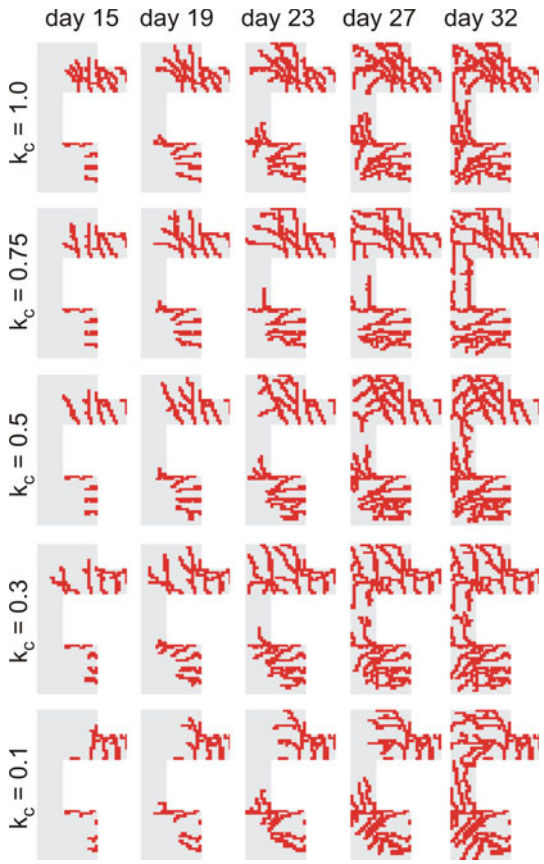

Fig. 8 Sensitivity to the relative importance of chemotaxis and haptotaxis. The evolution of the vasculature is shown for $k_c = 1$ (only chemotaxis, no haptotaxis), 0.75, 0.5, 0.3 and $k_c = 0.1$ (almost no chemotaxis)

murine femoral fracture. After 1 week the vasculature is limited. Only away from the fracture line, a few blood vessels of significant diameter are present, which is in agreement with the predictions of the mathematical model. The volume fraction of blood vessels in the callus is 0.4% (SD: 0.02%). One week later, the measured volume fraction is 2.8% (SD: 0.2%). As simulations are carried out in a 2D environment, the predicted blood vessel (surface) fractions can be up to a factor 3 higher than the experimentally measured 3D (volume) values due to the fact that the number of grid cells that are directly supplied of oxygen and nutrients by a single blood vessel is a factor 3 smaller in 2D versus 3D. With this constraint in mind, the prediction of the vasculature at PFW 1 is only a slight overestimation of the measured value, and the predicted fraction at PFW 2 is in agreement with the experimental result of Duvall et al. (2007).

In general, the hybrid model confirms that angiogenesis plays a major role in fracture healing. It should be remarked that the validation is still limited due to the fact that the model is two-dimensional. However, starting with the investigation of lower-dimensional models is a well-established approach in applied mathematics since geometric complexity and computational costs make the study of 3D versions much more involved (Ryser et al. 2009).

4.2 Convergence and sensitivity analyses

The convergence analysis indicates that the numerical method is stable. The grid dependence shown by the analysis is a result of the coupling between the blood vessel diameter and the grid cell size. As the description of tip cell movement is lattice-free in this model, only the projection of the blood vessels on the grid would need to be adapted to obtain fully grid-independent solutions.

The sensitivity analysis shows that the randomness of the fiber orientation gives rise to a controllable inter-simulation variability which does not affect general conclusions. The assumption of a random fiber orientation is appropriate, as only the reparative phase of fracture healing is modeled. Nevertheless, the approach allows to impose an alignment of matrix fibers which could be of use when the model is extended to simulate bone remodeling.

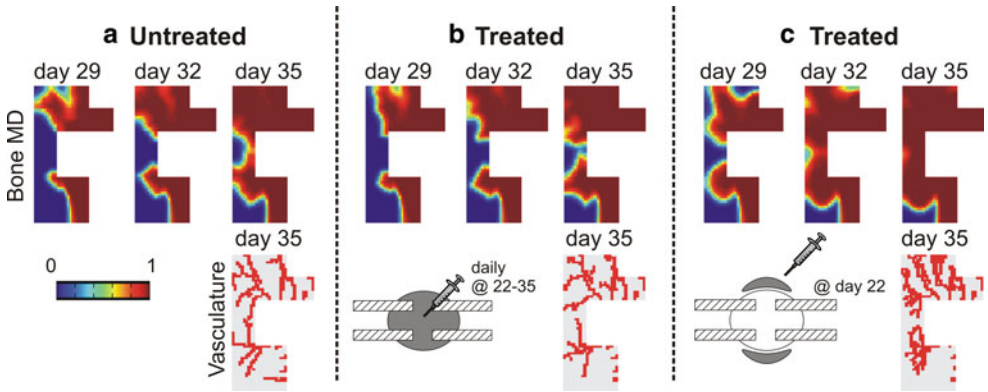

Fig. 9 Impaired endochondral ossification and treatment strategies: bone matrix density (MD, [×0.1 g/ml]) and vasculature; **a** delayed union; **b** daily VEGF bolus injections from postfracture day 22 onwards; **c** injection of a slow release VEGF-carrier on postfracture day 22

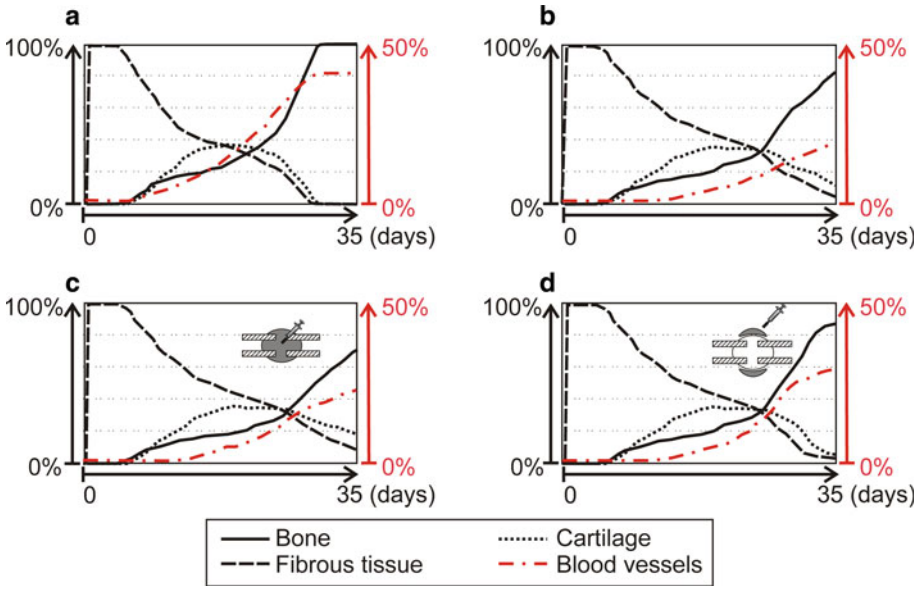

Fig. 10 Predicted temporal evolution of bone, cartilage and fibrous tissue fractions (%, axis on the left of each graph) and blood vessel density (%, axis on the right of each graph) in the callus; **a** normal fracture healing (Fig. 4); **b** impaired untreated fracture healing (Fig. 9a); **c** impaired fracture healing treated with VEGF bolus injections (Fig. 9b); **d** impaired fracture healing treated using a slow-release VEGF carrier (Fig. 9c)

Other simulations suggest that a fracture with severe initial vascular damage will still heal normally provided that there is a minimal supply of endothelial cells and that the few forming vessels are fully functional as assumed in the model.

The response of tip cells to chemotaxis and haptotaxis is very similar in this study. Chemotaxis is a result of a gradient in the vascular growth factor concentration. The principal source of this growth factor type are hypertrophic chondrocytes, which reside in dense cartilaginous tissue. Consequently, because of chemotaxis, tip cells will move to regions of high cartilaginous density. This is also where tip cells are directed to under influence of the haptotactic stimulus once the reparative healing phase has started, as the cartilaginous tissue gradient soon becomes greater than the fibrous tissue gradient.

4.3 Impaired fracture healing and treatment strategies

After corroboration, the presented model was used to simulate MMP9 deficiency, which correctly resulted in a delayed union. Whereas traditional therapies of impaired healing focus on mechanical stabilization of the fracture, new strategies try to influence the biological aspects of the healing, by administering VEGF among others (Colnot et al. 2003). The results of the simulations confirm that the retention time of the administered VEGF dose is crucial to the therapeutic effect of the treatment. However, the in silico findings are more pronounced than experiments suggest (Colnot et al. 2003). The model's theoretical value for the VEGF halftime seems to be too small to resort any effect in the case of the bolus strategy. This could be explained by a discrepancy of the theoretical VEGF half-time value and its actual retention time in living tissue.

4.4 Model limitations

This study has addressed some, but not all limitations of the model presented in Geris et al. (2008). Adaptations to the continuous model to simulate the influence of mechanical loading on the regeneration process are presented in Geris et al. (2010).

Because the geometry of the simulation domain is unmodified compared to Geris et al. (2008), the dorsoventral and mediolateral asymmetry of the femur is again not captured in the hybrid model. For the same reason there is still a need for boundary conditions on the osteogenic growth factors, osteoblasts and endothelial cells to account for processes taking place in the cortex and intact marrow.

Differentiation from one cell type to another is not modeled to go through any transitory state. Methods to incorporate this observation (Bruder and Scaduto 2005) into the model are suggested in Geris et al. (2008).

To fill up the lack of experimental data for the rodent bone regeneration model, parameters have been derived from a range of studies. Yet, it should be noted that changes to the experimental setup, e.g. an in vitro instead of in vivo situation, may affect the values of parameters of interest.

As was suggested by Geris et al. (2008), the adapted framework presented in this study recognizes the importance of oxygen and nutrients. However, in reality their role is even more extended than modeled here (see also Sect. 4.1).

Other valuable extensions to the framework would be to simulate the role of matrix metalloproteinases and the interactions between different growth factors.

Finally, as already pointed out in Sect. 3.1, the hybrid model is two-dimensional, forming a new limitation compared to the model of Geris et al. (2008). However, Gerisch and Geris (2007) indicate that the results for a 2D-simulation and for an axi-symmetric simulation only differ in a region close to the central axis.

4.5 Conclusion

This study presents the first mathematical model that simulates the biology of bone regeneration during fracture healing including a realistic, lattice-free description of endothelial tip cell migration and angiogenesis. The mechanoregulatory effects, which are present in the model of Checa and Prendergast (2008), are not yet incorporated here, but a framework to do this is already available (Geris et al. 2010). This study shows that a mathematical model can be a useful tool in the research of impaired healing and the design of treatment strategies.

Acknowledgments L.G. is a postdoctoral research fellow of the Research Foundation Flanders (FWO). This work is part of Prometheus, the Leuven Research & Development Division of Skeletal Tissue Engineering of the Katholieke Universiteit Leuven: http://www.kuleuven.be/prometheus. All the authors declare to have no conflict of interest.

Appendix

The continuous part of the hybrid bone fracture healing model consists of a nondimensionalized form of the Eqs. 1–11. The functional forms in these equations that have not been changed with respect to Geris et al. (2008) are summarized below. The other functional forms have been discussed in Sect. 2.2.

– *Random motion and haptokinesis* The random motion of mesenchymal stem cells was modeled as a haptokinetic process, based on Olsen et al. (1997). The resulting functional form is:

$$D_m = \frac{D_{\mathrm{hm}} m}{K_{\mathrm{hm}}^2 + m^2}.$$

– *Chemotaxis* Chemotaxis was modeled using a receptor-kinetic form, with a maximum response at a particular growth factor concentration as was observed in experiments (Lind et al. 1996; Fiedler et al. 2004, 2005; Metheny-Barlow et al. 2004). The resulting functional forms for chemotaxis of mesenchymal stem cells and fibroblasts are, respectively:

$$C_{m_{\mathrm{CT}}} = \frac{C_{\mathrm{kCTm}}(g_b + g_v)}{K_{\mathrm{kCTm}}^2 + (g_b + g_v)^2}$$

$$C_f = \frac{C_{\mathrm{kf}} g_b}{K_{\mathrm{kf}}^2 + g_b^2}.$$

– *Haptotaxis* The haptotactic coefficient was taken from Olsen et al. (1997), based on a kinetic analysis of a model mechanism for the cell-surface-receptor-extracellular ligand binding dynamics (Sherrat 1994). The resulting functional form is:

$$C_{m_{\mathrm{HT}}} = \frac{C_{\mathrm{kHTm}}}{(K_{\mathrm{kHTm}} + m)^2}.$$

– *Proliferation* Proliferation of cells was modeled by a logistic growth function (Olsen et al. 1997; Weinberg and Bell 1985; Yoshizato et al. 1985). The resulting functional forms are:

$$A_i = \frac{A_{\mathrm{i0}} m}{K_i^2 + m^2} \quad \text{for} \quad i = m, f, c, b.$$

– *Differentiation* The differentiation of mesenchymal stem cells toward chondrocytes was modeled to be mediated by the presence of chondrogenic growth factors with a saturation effect (Bailón-Plaza and Van der Meulen 2001). The resulting functional form is:

$$F_2 = \frac{Y_2 g_c}{H_2 + g_c}.$$

– *Production of growth factors* The production of chondrogenic and osteogenic growth factors by chondrocytes and osteoblasts, respectively, was modeled to level off at a certain saturation concentration. When chondrocytes become hypertrophic, they stop producing chondrogenic growth factors. The resulting functional forms are:

$$E_{\mathrm{gc}} = \frac{G_{\mathrm{gc}} g_c}{H_{\mathrm{gc}} + g_c} \times \frac{m}{K_{\mathrm{gc}}^3 + m^3}$$

$$E_{\mathrm{gb}} = \frac{G_{\mathrm{gb}} g_b}{H_{\mathrm{gb}} + g_b}.$$

The following scales were chosen for the nondimensionalization of the continuous model variables:

$$\tilde{t} = \frac{t}{T}, \quad \tilde{x} = \frac{x}{L}, \quad \tilde{y} = \frac{y}{L}, \quad \tilde{c_m} = \frac{c_m}{c_0}, \quad \tilde{c_f} = \frac{c_f}{c_0},$$

$$\tilde{c_c} = \frac{c_c}{c_0}, \quad \tilde{c_b} = \frac{c_b}{c_0}, \quad \tilde{m_f} = \frac{m_f}{m_0}, \quad \tilde{m_c} = \frac{m_c}{m_0},$$

$$\tilde{m_b} = \frac{m_b}{m_0}, \quad \tilde{g_c} = \frac{g_c}{g_0}, \quad \tilde{g_b} = \frac{g_b}{g_0}, \quad \tilde{g_v} = \frac{g_v}{g_0}, \quad \tilde{n} = \frac{n}{n_0}$$

where $T = 1\,\text{day}$, $L = 3.5\,\text{mm}$, $c_0 = 10^6\,\text{cells/ml}$, $m_0 = 0.1\,\text{g/ml}$, $g_0 = 100\,\text{ng/ml}$ and $n_0 = 39\,\text{mol/m}^3$.

The model parameters were nondimensionalized as follows (tildes referring to nondimensionalized parameters):

$$\begin{aligned}
\tilde{D}_{\text{hm}} &= \frac{D_{\text{hm}}T}{L^2 m_0} & \tilde{K}_{\text{hm}} &= \frac{K_{\text{hm}}}{m_0} & \tilde{C}_{\text{kCTm}} &= \frac{C_{\text{kCTm}}T}{L^2}\\
\tilde{K}_{\text{kCTm}} &= \frac{K_{\text{kCTm}}}{g_0} & \tilde{C}_{\text{kHTm}} &= \frac{C_{\text{kHTm}}T}{L^2 m_0} & \tilde{K}_{\text{kHTm}} &= \frac{K_{\text{kHTm}}}{m_0}\\
\tilde{A}_{\text{m0}} &= \frac{A_{\text{m0}}T}{m_0} & \tilde{K}_m &= \frac{K_m}{m_0} & \tilde{Y}_{11} &= Y_{11}T\\
\tilde{H}_{11} &= \frac{H_{11}}{g_0} & \tilde{Y}_{12} &= Y_{12}T & \tilde{H}_{12} &= \frac{H_{12}}{g_0}\\
\tilde{Y}_2 &= Y_2 T & \tilde{H}_2 &= \frac{H_2}{g_0} & \tilde{F}_4 &= F_4 T\\
\tilde{D}_f &= \frac{D_f T}{L^2} & \tilde{C}_{\text{kf}} &= \frac{C_{\text{kf}}T}{L^2} & \tilde{K}_{\text{kf}} &= \frac{K_{\text{kf}}}{g_0}\\
\tilde{A}_{\text{f0}} &= \frac{A_{\text{f0}}T}{m_0} & \tilde{K}_f &= \frac{K_f}{m_0} & \tilde{Y}_5 &= Y_5 T\\
\tilde{H}_5 &= \frac{H_5}{m_0} & \tilde{B}_v &= \frac{B_v}{m_0} & \tilde{B}_{\text{ec}} &= \frac{B_{\text{ec}}}{m_0}\\
\tilde{Y}_3 &= Y_3 T & \tilde{H}_3 &= \frac{H_3}{g_0} & \tilde{d}_f &= d_f\\
\tilde{A}_{\text{c0}} &= \frac{A_{\text{c0}}T}{m_0} & \tilde{K}_c &= \frac{K_c}{m_0} & \tilde{C}_{\text{kb}} &= \frac{C_{\text{kb}}T}{L^2}\\
\tilde{K}_{\text{kb}} &= \frac{K_{\text{kb}}}{g_0} & \tilde{A}_{\text{b0}} &= \frac{A_{\text{b0}}T}{m_0} & \tilde{K}_b &= \frac{K_b}{m_0}\\
\tilde{d}_b &= d_b T & \tilde{P}_{\text{fs}} &= \frac{P_{\text{fs}}Tc_0}{m_0} & \tilde{Q}_f &= Q_f m_0 c_0 T\\
\tilde{P}_{\text{cs}} &= \frac{P_{\text{cs}}Tc_0}{m_0} & \tilde{Q}_c &= Q_c c_0 T & \tilde{P}_{\text{bs}} &= \frac{P_{\text{bs}}Tc_0}{m_0}\\
\tilde{D}_{\text{gc}} &= \frac{D_{\text{gc}}T}{L^2} & \tilde{G}_{\text{gc}} &= \frac{G_{\text{gc}}Tc_0}{g_0 m_0^2} & \tilde{H}_{\text{gc}} &= \frac{H_{\text{gc}}}{g_0}\\
\tilde{K}_{\text{gc}} &= \frac{K_{\text{gc}}}{m_0} & \tilde{d}_{\text{gc}} &= d_{\text{gc}}T & \tilde{D}_{\text{gb}} &= \frac{D_{\text{gb}}T}{L^2}\\
\tilde{I}_v &= \frac{I_v}{m_0} & \tilde{G}_{\text{gb}} &= \frac{G_{\text{gb}}Tc_0}{g_0} & \tilde{H}_{\text{gb}} &= \frac{H_{\text{gb}}}{g_0}\\
\tilde{d}_{\text{gb}} &= d_{\text{gb}}T & \tilde{D}_{\text{gv}} &= \frac{D_{\text{gv}}T}{L^2} & \tilde{G}_{\text{gvb}} &= \frac{G_{\text{gvb}}Tc_0}{g_0 m_0^2}\\
\tilde{H}_{\text{gv}} &= \frac{H_{\text{gv}}}{g_0} & \tilde{K}_n &= \frac{K_n}{n_0} & \tilde{G}_{\text{gvc}} &= \frac{G_{\text{gvc}}Tc_0}{g_0 m_0^2}\\
\tilde{d}_{\text{gv}} &= d_{\text{gv}}T & \tilde{D}_n &= \frac{D_n T}{L^2} & \tilde{G}_n &= \frac{G_n c_0 T}{n_0}\\
\tilde{d}_n &= d_n T & \tilde{H}_n &= \frac{H_n}{n_0}.
\end{aligned}$$

This resulted in the following set of nondimensional parameter values:
$\tilde{D}_{\text{hm}} = 0.014$, $\tilde{K}_{\text{hm}} = 0.25$, $\tilde{C}_{\text{kCTm}} = 0.04$, $\tilde{A}_{\text{m0}} = 1.01$, $\tilde{K}_{\text{kCTm}} = 0.1$, $\tilde{C}_{\text{kHTm}} = 0.0034$, $\tilde{K}_{\text{kHTm}} = 0.5$, $\tilde{K}_m = 0.1$, $\tilde{\alpha}_m = 1$, $\tilde{Y}_{11} = 10$, $\tilde{H}_{11} = 0.1$, $\tilde{Y}_{12} = 2$, $\tilde{H}_{12} = 0.1$, $\tilde{Y}_2 = 50$, $\tilde{I}_v = 0.005$, $\tilde{H}_2 = 0.1$, $\tilde{F}_4 = 0.01$, $\tilde{D}_f = 0.02$, $\tilde{C}_{\text{kf}} = 0.4$, $\tilde{K}_{\text{kf}} = 0.1$, $\tilde{A}_{\text{f0}} = 0.202$, $\tilde{K}_f = 0.1$, $\tilde{\alpha}_f = 1$, $\tilde{Y}_5 = 50$, $\tilde{H}_5 = 0.1$, $\tilde{B}_v = 0.037$, $\tilde{B}_{\text{ec}} = 1.5$, $\tilde{Y}_3 = 1000$, $\tilde{H}_3 = 0.1$, $\tilde{d}_f = 0.1$, $\tilde{A}_{\text{c0}} = 0.101$, $\tilde{K}_c = 0.1$, $\tilde{\alpha}_c = 1$, $\tilde{C}_{\text{kb}} = 1.4 \cdot 10^{-8}$, $\tilde{K}_{\text{kb}} = 0.01$, $\tilde{A}_{\text{b0}} = 0.202$, $\tilde{K}_b = 0.1$, $\tilde{\alpha}_b = 1$, $\tilde{d}_b = 0.1$, $\tilde{P}_{\text{fs}} = 0.2$, $\tilde{\kappa}_f = 1$, $\tilde{Q}_f = 1.5$, $\tilde{P}_{\text{cs}} = 0.2$, $\tilde{\kappa}_c = 1$, $\tilde{Q}_c = 1.5$, $\tilde{P}_{\text{bs}} = 2$, $\tilde{\kappa}_b = 1$, $\tilde{D}_{\text{gc}} = 0.005$, $\tilde{G}_{\text{gc}} = 50$, $\tilde{H}_{\text{gc}} = 1$, $\tilde{K}_{\text{gc}} = 0.1$, $\tilde{d}_{\text{gc}} = 100$, $\tilde{D}_{\text{gb}} = 0.005$, $\tilde{G}_{\text{gb}} = 500$, $\tilde{H}_{\text{gb}} = 1$, $\tilde{d}_{\text{gb}} = 100$, $\tilde{D}_{\text{gv}} = 0.5$, $\tilde{G}_{\text{gvb}} = 0.005$, $\tilde{H}_{\text{gv}} = 15$, $\tilde{K}_n = 0.05$, $\tilde{G}_{\text{gvc}} = 5 \cdot 10^5$, $\tilde{d}_{\text{gv}} = 200$, $\tilde{d}_{\text{gvc}} = 1500$, $\tilde{D}_n = 0.014$, $\tilde{G}_n = 2$, $\tilde{d}_n = 18$, $\tilde{H}_n = 0.05$.

The value of the parameter $\tilde{D}_n$ was chosen so that the modeled diffusion coefficient of oxygen and nutrients represents only half the value measured by MacDougall and McCabe (1967). This scaling factor was introduced to account for the immediate functionality of the blood vessels in the model, which is not the case in reality as a first requirement is the formation of a lumen (De Smet et al. 2009). As the mathematical framework does not yet explicitly describe how oxygen and nutrients are supplied by means of blood flow and consumed by cells, the values of $\tilde{G}_n$ and $\tilde{d}_n$ were determined based on the results of a series of test simulations. They were chosen to give rise to a stable distribution of oxygen and nutrients in combination with the values of $\tilde{I}_v$, $\tilde{B}_v$, $\tilde{K}_n$ and $\tilde{H}_n$.

Finally, it can be noted that the values of $\tilde{G}_{\text{gvb}}$, $\tilde{G}_{\text{gvc}}$ and $\tilde{d}_{\text{gvc}}$ differ from those proposed in Geris et al. (2008), reflecting the change in the definition of c_v and the changes to the functional forms $\tilde{E}_{\text{gvb}}$ (Eq. 14) and $\tilde{E}_{\text{gvc}}$ (Eq. 15).

References

Anderson A, Chaplain M (1998) Continuous and discrete mathematical models of tumor-induced angiogenesis. Bull Math Biol 60: 857–900

Bailón-Plaza A, Van der Meulen M (2001) A mathematical framework to study the effects of growth factor influences on fracture healing. J Theor Biol 212:191–209

Barnes G, Kostenuik P, Gerstenfeld L, Einhorn T (1999) Growth factor regulation of fracture repair. J Bone Miner Res 14(11):1805–1815

Bernatchez P, Soker S, Sirois M (1999) Vascular endothelial growth factor effect on endothelial cell proliferation, migration, and platelet-activating factor synthesis is Flk-1-dependent. J Biol Chem 274(43):31,047–31,054

Bostrom M (1998) Expression of bone morphogenetic proteins in fracture healing. Clin Orthop Relat Res 355S:S116–S123

Bruder S, Scaduto T (2005) Cell-based strategies for bone regeneration: from developmental biology to clinical therapy. In: bone regeneration and repair. Humana Press, pp 67–92. doi:10.1385/1-59259-863-3:067

Carmeliet P, Jain R (2000) Angiogenesis in cancer and other diseases. Nature 407:249–257

Carter D, Beaupré G, Giori N, Helms J (1998) Mechanobiology of skeletal regeneration. Clin Orthop Relat Res 3558:S41–S55

Checa S, Prendergast P (2008) A mechanobiological model for tissue differentiation that includes angiogenesis: a lattice-based modeling approach. Ann Biomed Engin 37(1):129–145

Chen G, Niemeyer F, Wehner T, Simon U, Schuetz M, Pearcy M, Claes L (2009) Simulation of the nutrient supply in fracture healing. J Biomech 42(15):2575–2583

Claes L, Heigele C (1999) Magnitudes of local stress and strain along bony surfaces predict the course and type of fracture healing. J Biomech 32(3):255–266

Colnot C, Thompson Z, Miclau T, Werb Z, Helms J (2003) Altered fracture repair in the absence of MMP9. Development 130: 4123–4133

De Smet F, Segura I, De Bock K, Hohensinner P, Carmeliet P (2009) Mechanisms of vessel branching. Arter Thromb Vasc Biol 29: 639–649. doi:10.1161/ATVBAHA.109.185165

Dimitriou R, Tsiridis E, Giannoudis P (2005) Current concepts of molecular aspects of bone healing. Injury 36(12):1392–1404

Duvall C, Taylor W, Weiss D, Wojtowicz A, Guldberg R (2007) Impaired angiogenesis, early callus formation, and late stage

remodeling in fracture healing of osteopontin-deficient mice. J Bone Miner Res 22(2):286–297
Fiedler J, Etzel N, Brenner R (2004) To go or not to go: migration of human mesenchymal progenitor cells stimulated by isoforms of PDGF. J Cell Biomech 93:990–998
Fiedler J, Leucht F, Waltenberger J, Dehio C, Brenner R (2005) VEGF-A and PlGF-1 stimulate chemotactic migration of human mesenchymal progenitor cells. Biochem Biophys Res Comm 334: 561–568
Geris L, Gerisch A, Vander Sloten J, Weiner R, Van Oosterwyck H (2008) Angiogenesis in bone fracture healing: a bioregulatory model. J Theor Biol 25:137–158
Geris L, Vander Sloten J, Van Oosterwyck H (2010) Connecting biology and mechanics in fracture healing: an integrated mathematical modeling framework for the study of nonunions. Biomech Model Mechanobio. doi:10.1007/s10237-010-0208-8
Gerisch A, Chaplain M (2006) Robust numerical methods for taxis-diffusion-reaction systems: applications to biomedical problems. Math Comput Model 43:49–75
Gerisch A, Geris L (2007) Advances in mathematical modeling of biological systems, vol 1, Deutsch A, Brusch L, Byrne H, de Vries G, Herzel H-P, Boston, chap A finite volume spatial discretisation for taxis-diffusion-reaction systems with axi-symmetry: application to fracture healing. pp 303–316
Gerstenfeld L, Cullinane D, Barnes G, Graves D, Einhorn T (2003) Fracture healing as a post-natal developmental proces: molecular, spatial, and temporal aspects of its regulations. J Cell Biochem 88:873–884
Harrison L, Cunningham F, Srömberg L, Goodship A (2003) Controlled induction of a pseudarthrosis: a study using a rodent model. J Orthop Trauma 17:11–21
Hirao M, Tamai N, Tsumaki N, Yoshikawa H, Myoui A (2006) Oxygen tension regulates chondrocyte differentiation and function during endochondral ossification. J Biol Chem 291(41):31,079–31,092
Lind M, Eriksen E, Bunger C (1996) Bone morphogenetic protein-2 but not bone morphogenetic protein-4 and 6 stimulates chemotactic migration of human osteoblasts, human marrow osteoblasts and U2-OS cells. Bone 18:53–57
MacDougall J, McCabe M (1967) Diffusion coefficient of oxygen through tissues. Nature 215:1173–1174
Marsh D (1998) Concepts of fraction union, delayed union, and nonunion. Clin Orthop Relat Res S355:S22–S30
Mayer H, Bertram H, Lindenmaier W, Korff T, Weber H, Weich H (2005) Vascular endothelial growth factor (VEGF-A) expression in human mesenchymal stem cells: autocrine and paracrine role on osteoblastic and endothelial differentiation. J Cell Biochem 95:827–839
Metheny-Barlow L, Tian S, Hayes A, Li L (2004) Direct chemotactic action of angiopoietin-1 on mesenchymal cells in the presence of VEGF. Microvasc Res 68:221–230
Midy V, Plouet J (1994) Vasculotropin/vascular endothelial growth factor induces differentiation in cultured osteoblasts. Biochem Biophys Res Comm 199:380–386
Milde F, Bergdorf M, Koumoutsakos P (2008) A hybrid model for three-dimensional simulations of sprouting angiogenesis. Biophys J 95:3146–3160
Olsen L, Sherratt J, Maini P, Arnold F (1997) A mathematical model for the capillary endothelial cell-extracellular matrix interactions in wound-healing angiogenesis. IMA J Math Appl Med Biol 14: 261–281
Qutub A, Popel A (2009) Elongation, proliferation & migration differentiate endothelial cell phenotypes and determine capillary sprouting. BMC Syst Biol 3(13). doi:10.1186/1752-0509-3-13
Ryser M, Nigam N, Komarova S (2009) Mathematical modeling of spatio-temporal dynamics of a single bone multicellular unit. J Bone Miner Res 24(5):860–870
Seeherman H, Li R, Wozney J (2003) A review of preclinical program development for evaluating injectable carriers for osteogenic factors. J Bone Joint Surg 85:96–108
Shefelbine S, Augat P, Claes L, Simon U (2005) Trabecular bone fracture healing simulation with finite element analysis and fuzzy logic. J Biomech 38(12):2440–2450
Sherrat J (1994) Chemotaxis and chemokinesis in eukaryotic cells: the keller-segel equations as an approximation to a detailed model. Bull Math Biol 56:129–146
Street J, Bao M, deGuzman L, Bunting S, Peale FJ, Ferrara N, Steinmetz H, Hoeffel J, Cleland J, Daugherty A, van Bruggen N, Redmond H, Carano R, Filvaroff E (2002) Vascular endothelial growth factor stimulates bone repair by promoting angiogenesis and bone turnover. PNAS 99(15):9656–9661
Sun S, Wheeler M, Obeyesekere M, Patrick CJ (2005) A deterministic model of growth factor-induced angiogenesis. Bull Math Biol 67:313–337
Taguchi K, Ogawa R, Migata M, Hanawa H, Ito H, Orimo H (2005) The role of bone marrow-derived cells in bone fracture repair in a green fluorescent protein chimeric mouse model. Biochem Biophys Res Comm 331:31–36
Weinberg C, Bell E (1985) Regulation of proliferation of bovine aortic endothelial cells, smooth muscle cells and adventitial fibroblasts in collagen lattices. J Cell Physiol 122:410–414
Weiner R, Schmitt B, Podhaisky H (1997) ROWMAP—a ROW-code with Krylov techniques for large stiff ODEs. Appl Numer Math 25:303–319
Yoshizato K, Taira T, Yamamoto N (1985) Growth inhibition of human fibroblasts by reconstituted collagen fibrils. Biomed Res 6:61–71